AIAA JOURNAL
Vol. 56, No. 7, July 2018

Ensemble-Based State Estimator for Aerodynamic Flows

Andre F. C. da Silva* and Tim Colonius†
California Institute of Technology, Pasadena, California 91101

DOI: 10.2514/1.J056743

Regardless of the plant model, robust flow estimation based on limited measurements remains a major challenge in successful flow control applications. Aiming to combine the robustness of a high-dimensional representation of the dynamics with the cost efficiency of a low-order approximation of the state covariance matrix, a flow state estimator based on the ensemble Kalman filter is applied to two-dimensional flow past a cylinder and an airfoil at high angle of attack and low Reynolds number. For development purposes, the numerical algorithm is used as both the estimator and as a surrogate for the measurements. Estimation is successful using a reduced number of either pressure sensors on the surface of the body or sparsely placed velocity probes in the wake. Because the most relevant features of these flows are restricted to a low-dimensional manifold of the state space, asymptotic behavior of the estimator is shown to be achieved with a small ensemble size. The relative importance of each sensor location is evaluated by analyzing how they influence the estimated flowfield, and optimal locations for pressure sensors are determined. Covariance inflation is used to enhance the estimator performance in the presence of unmodeled freestream perturbations. A combination of parametric modeling and augmented state methodology is used to successfully estimate the forces on immersed bodies subjected to deterministic and random gusts.

I. Introduction

THE agility, endurance, and maneuverability of the next-generation aircraft could be enhanced if they could tolerate a broad spectrum of gusts while safely performing maneuvers that would otherwise lie outside of the flight envelope. Closed-loop control techniques might yet achieve these goals, but a pacing item in deploying them is our ability to robustly estimate the flow state from the available measurement data such as pressure readings on the wings and fuselage [1].

Although several state estimation techniques have been developed, their application to fluid dynamics is challenging due to the nonlinearity and high dimensionality of the underlying physical phenomena. Fluid systems are represented by spatially continuous models, and any suitable discretization results in high-dimensional discrete models. Whereas feedback control applications require real-time state estimation, the computational cost of standard control techniques such as the Kalman filter [2] does not scale well with increasing flow complexity and faster time scales. Also, numerical simulations require appropriate boundary and initial conditions that are uncertain [3]. Measurement data can provide the necessary information to close the gap between simulation and experiments. The development of methodologies for the seamless integration of measurement data and (often sophisticated) mathematical models is the goal of a research area known as data assimilation.

Within the flow control community, the most common approach to reduce computational cost is the development of reduced-order models (ROMs). Provided that these models have a low number of degrees of freedom, the classical control techniques become feasible. Gerhard et al. [4] use a three-mode proper orthogonal decomposition (POD)–Galerkin model (enhanced with the shift mode) to design a control to suppress the vortex shedding behind circular cylinders at low Reynolds numbers. Aleksic et al. [5] use data from 15 pressure sensors and a five-mode Galerkin model to decrease and stabilize the drag of a two-dimensional (2-D) bluff body. Ahuja and Rowley [6] used a 22-mode ROM obtained by balanced truncation to design an Linear-quadratic-Gaussian controller for the flow past an inclined flat plate. Flinois and Morgans [7] used the eigenvalue realization algorithm to construct an unstable 10-mode ROM, which was then used to design $\mathcal{H}_\infty$ controllers to stabilize the system. These ROMs, however, are fragile with respect to initial conditions and flow parameters like the Reynolds number. Alternatively, researchers such as Fukumori and Malanotte-Rizzoli [8] and Suzuki [9] proposed the use of reduced-order approximations to the Kalman filter that restrict the correction to the larger scales of the solution and alleviate the computational cost involved.

On the other hand, researchers in fields such as meteorology, oceanography, and geophysical fluid dynamics have developed data assimilation algorithms that are inherently capable of dealing with high-dimensional nonlinear systems and high volumes of measurement data [10,11]. These methods take full advantage of the increasingly available computational power and efficient parallel implementations and had not, until recently, received much attention from the flow control community. Colburn et al. [12] applied an ensemble Kalman filter (EnKF) to the problem of estimating the statistics of the three-dimensional turbulent channel flow. Kikuchi et al. [13] compared the performance of an EnKF and a particle filter applied to the POD–Galerkin model of the problem of the flow past a cylinder. Kato et al. [14] used a variation of the EnKF to achieve synchronization between a Reynolds-averaged Navier–Stokes/Spalart–Allmaras numerical simulation of a steady transonic flow past airfoils and pressure experimental data. Mons et al. [15] use a Kalman smoother and other variational methods to reconstruct freestream perturbation history based on measurements taken on and around a circular cylinder subjected to it.

A well-known alternative for sequential data assimilation of high-dimensional systems is the 3D-Var [16]. Just like the Kalman filter, 3D-Var can be formulated as an observer in which the gain is calculated to minimize a cost function, with the general format

$$J(x) = [y_0 - h(x)]^T R^{-1}[y_0 - h(x)] + [x - x_f]\Sigma^{-1}[x - x_f] \quad (1)$$

where y_0 is the measurement taken from the tracked system, x_f is the prior estimate for the state, $h(x)$ is the observation function, and R is a weighting matrix associated to the measurement mismatch. The main difference is that 3D-Var regards Σ as a predefined constant weight matrix, whereas the EnKF regards it as an ensemble-based approximation to the true state covariance matrix. Because just a single estimate must be propagated, 3D-Var is far less computationally demanding than EnKF. However, estimator performance depends

Presented as Paper 2017-3483 at the 8th AIAA Theoretical Fluid Mechanics Conference, Denver, CO, 5–9 June 2017; received 25 September 2017; revision received 15 January 2018; accepted for publication 4 March 2018; published online 28 May 2018.

*Graduate Student, Division of Engineering and Applied Science, Department of Mechanical and Civil Engineering; andrefcs@caltech.edu.

†Frank and Ora Lee Marble Professor of Mechanical Engineering, Division of Engineering and Applied Science, Department of Mechanical and Civil Engineering. Associate Fellow AIAA.

heavily on the a priori choice of Σ. The EnKF is irrefutably suboptimum in the presence of nonlinearities, but Kalman's rule provides at least a consistent way of estimating Σ on the fly by taking into account relevant information about the dynamics.

In this paper, we employ an EnKF to estimate the state of flow past a body from pressure measurements on the surface or sparse velocity measurements in the flowfield. In Sec. II, a brief description of the algorithm is presented. In Sec. III, we show some results of the application of the method to the flow past a circular cylinder and a NACA 0009 airfoil at high angle of attack. Finally, Sec. IV enumerates some conclusions.

II. Ensemble Kalman Filter

Consider an input/output discrete-time system modeled by

$$x_{k+1} = f_k(x_k, u_k) + g_k(x_k)\omega_k \tag{2a}$$

$$y_k = h(x_k) + \nu_k \tag{2b}$$

where f_k is a general function of the n-dimensional state x_k and the control input u_k; $g(x)$ represents the dependence of the process noise on the state; ω_k accounts for state disturbances and process noises; $h(x)$ is the measurement function (y_k is a p-dimensional vector); and ν_k represents sensor noise. The subscript k refers to quantities taken at time $t = t_k$. We also assume that both ω_k and ν_k are zero-mean, Gaussian, and white random processes [$\omega_k \sim N(0, Q_k)$ and $\nu_k \sim N(0, R_k)$] that are uncorrelated in time ($E[\omega_k\omega_l^T] = Q_k\delta_{kl}$ and $E[\nu_k\nu_l^T] = R_k\delta_{kl}$).

The goal of the filtering process is to use measurement data to construct an estimate of the state x_k, denoted by $\hat{x}_k$, which is optimal in the sense that it minimizes the estimation variance (or, equivalently, maximizes the likelihood) [17]. The fundamentals of optimal filtering were derived by Kalman and Bucy in 1961 [2]. The classical Kalman filter (KF) provides the optimum solution for the state estimation of linear systems under Gaussian-distributed noise. Within this context, the estimate for the state x is regarded as a Gaussian-distributed random variable with mean $\hat{x}$ and covariance Σ.

Devising an optimal state estimator for systems exhibiting nonlinear dynamics using measurement data that are a nonlinear function of the state is more challenging. Rigorous solutions to the estimation problem for nonlinear systems are typically either narrow in applicability or computationally infeasible [18]. For weakly nonlinear cases, the extended Kalman filter [19] is considered the standard technique. Nevertheless, its robustness and reliability are impaired by the linearization process, and Julier and Uhlmann [20] showed that even the near-ubiquitous nonlinear transformation from polar to Cartesian coordinates is enough to yield significant deviations in tracking the correct state. For cases where there are strong nonlinearities, the unscented Kalman filter tends to deliver better results [21]. For all these KF variants, the cost of the propagation of the covariance matrix Σ is in the order of n evaluations of the forecast operator and becomes quickly prohibitive for large systems.

Under nonlinear dynamics, the probability density function (PDF) of the estimate need not remain Gaussian, and the first two moments cease to fully represent the state. Instead, the full PDF could, in principle, be propagated through time using a suitable discretization of the Fokker–Plank equation yielding a class of schemes known as particle filters [12,22]. Because they rely on the direct sampling of an n-dimensional state space, the curse of dimensionality [23] is severe for these techniques, and they are only computationally tractable for systems of reduced dimension.

Aiming at overcoming the cost barrier, in 1994 Evensen [24] proposed a Monte Carlo approximation to the KF in which the internal state of the estimator is represented by an ensemble of particles so that the corresponding ensemble mean and covariance matrix are used to approximate $\hat{x}$ and Σ. This method was named ensemble Kalman filter (EnKF) and, since then, has been extensively used for high-dimensional systems (thousands of degrees of freedom or more) associated with a computationally onerous forecast (as in meteorology, oceanography, and geophysical flows [25–27]). In such context, this technique has shown to provide a correct estimate of the first two moments of state of the system even for a small ensemble size (provided that the Gaussian assumption appears to hold) [28].

Consider an ensemble of q initially independent states. The expected value of the system state corresponds to the ensemble average of these states:

$$\bar{x}_k = \frac{1}{q}\sum_{j=1}^{q} \hat{x}_k^j \tag{3}$$

Defining the error matrix E_k^s as

$$E_k^s = [\hat{x}_k^1 - \bar{x}_k \ldots \hat{x}_k^q - \bar{x}_k] \tag{4}$$

and the output error matrix E_k^o as

$$E_k^o = [\hat{y}_k^1 - \bar{y}_k \ldots \hat{y}_k^q - \bar{y}_k] \tag{5}$$

where $\hat{y}_k^j = h(\hat{x}_k^j)$ and $\bar{y}_k$ is the ensemble average of the outputs, one can finally compute the ensemble covariance matrix

$$\Sigma_k = \frac{1}{q-1} E_k^s (E_k^s)^T \tag{6}$$

which is an estimate of the state covariance matrix.

The filtering process can be synthesized in two steps [18,29].

1) Dynamic update (or forecast step): The state of each ensemble member at the next time step is estimated using the (possibly nonlinear) dynamic model [Eq. (2a)]:

$$\hat{x}_{k+1|k}^j = f(\hat{x}_{k|k}^j, u_k) + g(\hat{x}_{k|k}^j)\eta_k^j \tag{7}$$

If applied to a linear system, this ensemble approach reduces the cost associated with the time propagation of the covariance matrix from $\mathcal{O}(n^3)$ (classical KF) to $\mathcal{O}(n^2 q)$ (EnKF). Because typical ensemble sizes are no larger than $\mathcal{O}(10^2)$, the overall cost is usually reduced by several orders of magnitude.

2) Measurement update (or analysis step): The ensemble members are corrected to minimize the error with respect to the measurements in the presence of noise and model uncertainties. An efficient way to implement the measurement update step is by using the representers' formulation proposed by Evensen and Van Leeuwen [30]:

$$\hat{x}_{k+1|k+1}^j = \hat{x}_{k+1|k}^j + \Sigma_{k+1} H_{k+1}^T b_{k+1}^j \tag{8}$$

where the columns of $\Sigma_{k+1}H_{k+1}^T$ are called the representers and represent the influence vectors for each measurement. The vector b_k^j then represents the magnitude by which each of the representers actuates in $\hat{x}$. It can be obtained as the solution to the linear system:

$$(H_k \Sigma_k H_k^T + R_k) b_k^j = y_k^j - h(x_k^j) \tag{9}$$

Each y_k^j must be independently sampled from a normal distribution whose mean is the measurement vector obtained from the estimated system and whose variance is R_k. Because of this sampling step, this algorithm is often referred to as perturbed observations (or stochastic) EnKF. Although this procedure introduces an additional sampling error, previous work by Lawson and Hansen [31] suggested that it performs better in the presence of nonlinearities than its deterministic alternatives.

The subscript $m|n$ is used to denote a random variable taken at time t_m that has assimilated measurement data up to time t_n. It is worthy to note that one never needs to explicitly evaluate Σ_k because it suffices to evaluate

$$\Sigma_k H_k^T = \frac{1}{q-1} E_k^s (E_k^o)^T \quad \text{and} \quad H_k \Sigma_k H_k^T = \frac{1}{q-1} E_k^o (E_k^o)^T \tag{10}$$

Both the particle filter (PF) and the EnKF algorithms share the same forecast step, but their analysis steps are distinct. Although in

the PF the posterior PDF corresponds to a linear combination of the prior ensemble whose weights are calculated using Bayes's rule, the EnKF assign equal weights to all particles and correct the ensemble members themselves according to Kalman's update rule.

Because the KF assumes model linearity and that all probability distributions are Gaussian, optimality can only be expected as $q \to \infty$, provided that these hypotheses hold. Under nonlinear dynamics, this suboptimum filter can only be expected to provide estimates for the first two moments of a possible general state PDF. In fact, Le Gland et al. [32] demonstrated that, in general, the EnKF exhibits a $q^{-1/2}$ rate of convergence to the estimate asymptotic PDF. However, this limiting distributing may differ of the optimum filtering distribution because the optimum filtering solution may be multimodal or exhibit other higher-order features in the presence on nonlinearities.

In a practical setting, the ensemble size q required to guarantee the filter convergence will depend on the effective state space dimension (the dimensionality of the manifold in which the most relevant dynamics in confined) and on our ability of recognizing and sampling this meaningful part of the state space [28]. Nevertheless, typical ensemble sizes do not exceed a few hundred in view of the available computational power, and for such small ensemble sizes, the EnKF exhibits some interesting characteristics.

First, because the correction added to each ensemble member during the analysis step is a combination of the forecast ensemble states, the analysis step operates only in the subspace spanned by the ensemble at hand [33]. Therefore, the choice of initial ensemble can limit, at least initially, the effectiveness of the correction applied by the estimator to the ensemble members.

Also, small ensemble sizes lead to systematically underestimated error covariances [34]. For a fixed measurement noise level, as the estimated covariance decreases, the weight given to the measurement data in the analysis step decreases and eventually becomes negligible. This phenomenon may lead to the divergence of the estimator and is known as covariance collapse, in reference to the fact that the particles collapse onto a single trajectory. The most common empirical algorithm fix is covariance inflation (CI). This technique artificially increases the ensemble covariance to weight the measurement data more heavily. Kelly et al. [35] showed that, for a large enough inflation, the boundedness of the EnKF can be guaranteed.

In general, the covariance inflation can be implemented as

$$\hat{x}^j = \bar{x} + \beta(\hat{x}^j - \bar{x}) + \alpha^j \tag{11}$$

where α^j is the additive covariance inflation vector that is usually drawn from a zero-mean normal distribution with covariance S, and β is the multiplicative covariance inflation parameter. Whitaker and Hamill [36] suggested that multiplicative inflation is especially useful in capturing the pernicious effects of the sampling errors associated with a small ensemble, whereas additive inflation seems to be most effective in capturing sources of error that do not depend on the assimilation process such as the system modeling error. However, any practical implementation of an additive scheme requires prior knowledge of this modeling error (namely, a way of producing the matrix S). Multiplicative CI can delay the collapse of the covariance, whereas using additive CI will enforce a lower bound to the system covariance. In addition, the inflation parameter must be chosen carefully to avoid a divergent result.

The simplest multiplicative covariance inflation scheme is the one suggested by Anderson and Anderson (AA) [27], in which β is a scalar (typically, $\beta \in [1.005, 1.05]$). This scheme corresponds to using $g_k(x_k) = \sqrt{\Sigma_k}$. After analyzing the effect of sampling errors introduced by limited-size ensembles, Sacher and Bartello [37] concluded that more inflation is needed when observations lead to large corrections to the estimate. Later, Whitaker and Hamill [36] proposed an inflation scheme termed relaxation-to-prior spread (RTPS). In this case, β takes the form of the vector

$$\beta_i = 1 + \theta\left(\frac{\sigma_i^b - \sigma_i^a}{\sigma_i^a}\right) \tag{12}$$

where θ is a scalar (typically, $\theta \in [0.5, 0.95]$), and σ_i^b and σ_i^a are, respectively, the prior and posterior ensemble standard deviation for the ith state variable. Note that because β is now a vector, its multiplication with the perturbation vector $(\hat{x}^j - \bar{x})$ must be performed component-wise.

Because the AA scheme results in particles that are linear combinations of the previous ones, they will naturally satisfy any kinematic constraints (boundary conditions). That is not the case with the RTPS scheme, which may yield nonconforming particles because each state variable is updated independently. In this particular implementation, the nonconforming parts of the solutions are projected out using the numerical method discussed in the next section.

III. Numerical Experiments

The dynamics of the flow is represented by the discretized 2-D incompressible Navier–Stokes equations, and the simulations were carried out using the immersed boundary projection method [38,39] enhanced by the lattice Green's function (LGF) formulation [40,41]. The LGF formulation enforces exactly the free-space boundary condition at infinity even though the computation domain is restricted to the region of nonzero vorticity near the immersed body. The integrating factor approach is also used in conjunction with the LGF formulation to avoid the stiffness introduced by the viscous terms in the Navier–Stokes equation. Finally, a half-explicit Runge–Kutta scheme, specially suitable to deal with systems of ODEs with algebraic constraints, is used as the time marching scheme.

In addition to dynamically updating the ensemble members, this numerical solver is also used to generate the base solution and to collect the measurement data that were used for estimation purposes. This solution is regarded as the true state of the system that the estimator is supposed to track.

The initialization of the estimator plays a crucial role in its performance. Theoretically, to completely span an n-dimensional state space, one would need at least n ensemble members. Instead, the initial ensemble is constructed using the improved sampling scheme proposed by Evensen [10]. Starting from a dataset of snapshots of the base solution throughout 20 convective time units, the base mean flow $\bar{x}_b$ and the leading proper orthogonal decomposition (POD) modes are computed. Then, the q ensemble members are randomly sampled from the subspace spanned by the first q POD modes of the data so that the ensemble average is $\bar{x}_b$ and the norm of ensemble covariance matrix matches the norm of the dataset covariance matrix. If the first few POD modes concentrate most of the energy of the flow, this sampling technique allows a more efficient distribution of the initial states.

To evaluate the performance of the estimator, the following metrics will be used.

1) Estimate error measures how the estimated state differs from the reference state:

$$E_x = \frac{\|\bar{x} - x_b\|}{\|x_b\|} \tag{13}$$

2) Ensemble state rms measures the spread of the ensemble:

$$\mathrm{RMS}_x = \sqrt{\frac{1}{q-1}\sum_{i=1}^{q}\frac{\|x_i - \bar{x}\|^2}{\|\bar{x}\|^2}} \tag{14}$$

A. Perfect Model Estimation

The estimator performance will be significantly impacted by the choice of how to model and observe the tracked system. The definition of the predictive model must be a compromise between accuracy and cost. The predictive model should be accurate enough to alleviate the burden laid upon the error control techniques (stochastic forcing, covariance inflation, etc.) while keeping the computational time expenditure controlled. On the other hand, the choice of what and where to measure not only limits the accuracy of

the state/output estimates but also determines if the estimation task is feasible at all (detectability).

In this subsection, we discuss how tuning the different estimation parameters affects the performance of the estimator in a perfect model framework. We show that the representers of the estimator [defined in Eq. (8)] provide guidance on sensor placement.

1. *Flow past a Circular Cylinder*

The first test case is the canonical flow past a circular cylinder at $Re_D = 100$. At this Reynolds number, the flow is still essentially two-dimensional [42] and is characterized by the existence of coherent vortices in the wake known as the Karman vortex street. The dynamical system is deterministic, and apart from synthetic noise added to the measurements, the only randomization is associated with the initial conditions. The goal is to use the EnKF to track the phase of the vortex street.

The grid resolution is 25 points by diameter (which yields a system with about 15,000 degrees of freedom), and velocity components sampled at 14 equidistant points in the flowfield (see Fig. 1) are assimilated into the filtering process every 0.1 convective time units. The AA covariance inflation scheme with $\beta = 1.05$ is used.

Figure 2 shows how different choices of the initial ensemble impact the evolution of the estimate error when the ensemble size is held fixed at 24 members. In the first case, we initialize the flowfield with zero-mean random numbers, whereas in the second case, we add random perturbations to the true mean flow. Finally, in the third case, we add the first 24 POD modes to the mean, but with coefficients randomized. In all cases, the ensemble initial variance matches the reference run variance. When the initial condition is restricted to the POD subspace, the estimator convergences within a few convective time units, whereas, unsurprisingly, the more random initial conditions take longer to converge. Physically speaking, the time scale associated with the domain size in the x direction is about six units, and the estimator must wash out the random initial condition over this time period while a transient takes place that leads to different realizations of the flow with distinct vortex shedding phases.

Fig. 1 Flow past a circular cylinder: location of the velocity measurement points in the flowfield.

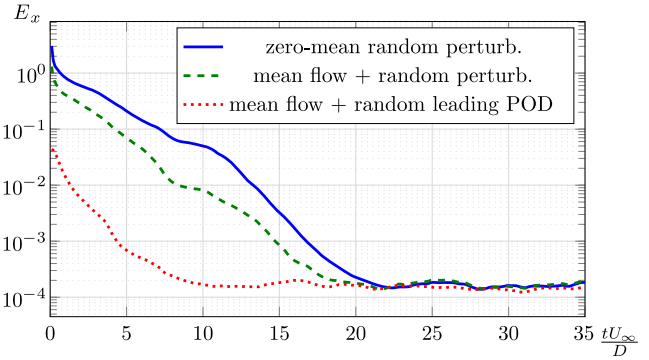

Fig. 2 Effect of the choice of the initial ensemble on the estimator performance for the flow past a circular cylinder at $Re = 100$ using velocity measurements. Measurement error level is $R = 10^{-4} I_p$.

Figure 3 presents the evolution of the state estimate error and ensemble rms for different ensemble sizes. Provided that the dynamics is relatively sparse in the POD space and the most energetic subspace is captured by the initial ensemble, the transient behavior of the estimator appears to become independent of the ensemble size. This behavior indicates that the sampling error decays more rapidly than the expected $q^{-1/2}$ when a POD-based initialization is used. Another interesting behavior that is portrayed in these plots is the collapse of the variance. For smaller ensemble sizes, the ensemble rms decreases rapidly limiting the effectiveness of further corrections to the state as the confidence on the internal state is overestimated. As a consequence, error converges in a slower rate than when more ensemble members are used. However, if modeling errors were present, the increasing disregard for new external information coming from the measured data may lead the estimator to diverge.

The measurement noise level also impacts the performance of the estimator because the reliability of sensor data should be weighted against the internal state of the estimator. As the data assimilation proceeds, the estimated state uncertainty decreases and may reach an error level for which further corrections become secondary. Figure 4 shows how a lower noise level favors the estimator performance. Note that reducing the noise covariance level by two orders of magnitude reduces the ensemble rms by one order of magnitude, as expected.

Figure 5 shows the measurement influence fields (representers) for different measurement locations, as defined in Eq. (8). Each of these vectors comprises two pieces of information; its magnitude provides a comparative measure on how strongly the data gathered from each of the sensors contributes to the correction, and its shape shows where in the flowfield these corrections take place. The highest values are achieved for measurements taken about two diameters downstream of the cylinder. The obvious conclusion is that measurements taken at points where there is no variation amongst the ensemble members are useless. Interestingly, the region of highest influence is coincident with the so-called wave-maker region [43].

2. *Flow past a NACA 0009 Airfoil at High Angle of Attack*

The second test case is closer to the motivation presented in Sec. I. The performance of the estimator is now analyzed when applied to the problem of the flow past a NACA 0009 at 30 deg angle of attack and Reynolds number 200. The grid resolution is 50 points per chord, and the pressure at distinct locations over the airfoil is taken as measurement data every 0.05 convective time units. The ensemble size was set to 24 in all cases. The estimator is able to track the vortex shedding phase with as few as 10 measurements locations (see Fig. 6).

Figure 7 shows the estimated lift coefficient evolution with the RTPS scheme ($\theta = 0.95$). The behavior of the ensemble members can be analyzed using Eq. (9). Before the first analysis step, the variation of the ensemble predicted measurements $H_k \Sigma_k H_k^T$ is much larger than the measurement noise level R_k. As a consequence, all ensemble members are strongly corrected toward the true solution in the first time step. At subsequent times, corrections are increasingly damped as the estimate converges to the true flow state and the measurement variance across the ensemble decreases.

We now analyze the effect of using different choices of covariance inflation (CI) scheme. These schemes delay the decreasing trend of the ensemble covariance (see Figs. 8c and 8d) and, as a consequence, achieve a smaller error than the one obtained without inflation (see Figs. 8a and 8b). Because a constant factor is used to inflate the covariance in the AA scheme, the error subspace spanned by the ensemble is preserved. The corrections in this case are structurally similar to those that would have taken place in the absence of inflation but are more aggressive. The RTPS scheme, on the other hand, is more complex. The inflation magnitude is local and dependent upon the previous analysis step (for $\theta = 1$, the forecast spread is recovered). Because of these characteristics, the RTPS scheme can, in fact, change the subspace spanned by the ensemble. This extra variability is possibly the reason for the distinct behavior at early times and may be even desirable for some applications.

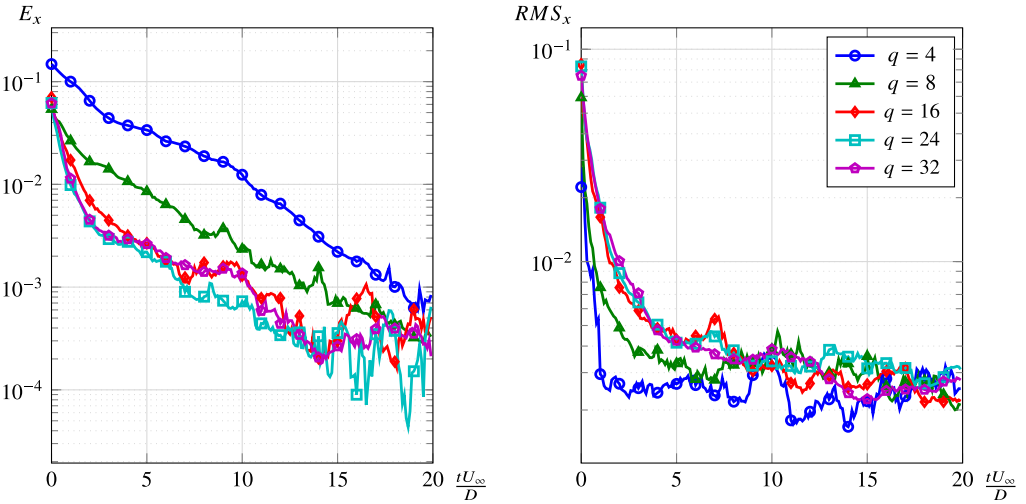

a) State estimate error b) Ensemble RMS

Fig. 3 Estimator performance for increasing ensemble sizes applied to the problem of the flow past a circular cylinder at $Re = 100$ using velocity measurements. Measurement error level is set to $R = 10^{-4} I_p$.

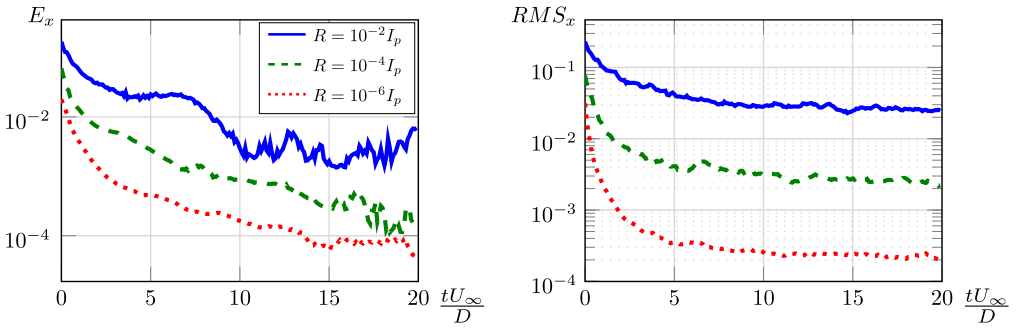

a) State estimate error b) Ensemble RMS

Fig. 4 Estimator performance for distinct measurement noise levels applied to the problem of the flow past a circular cylinder at $Re = 100$ using velocity measurements and 16 ensemble members.

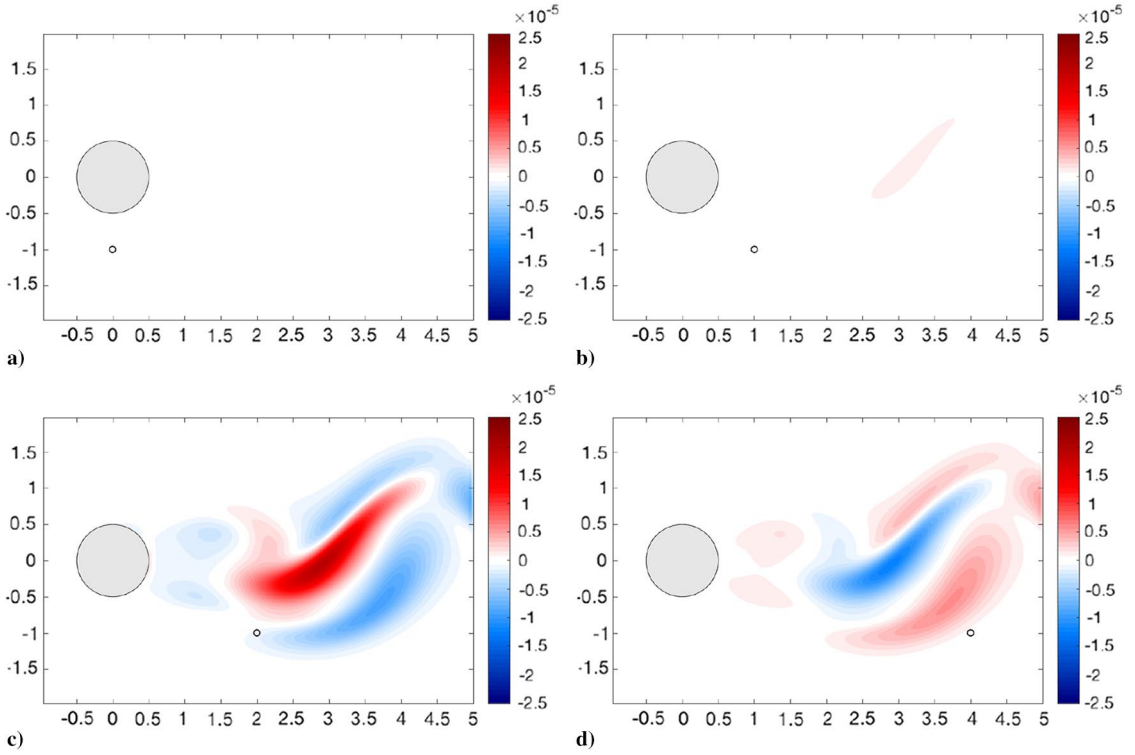

Fig. 5 Measurement influence fields (representers) for the horizontal component of the fluid velocity at selected measurement locations. Ensemble size was 16 members, and $R = 10^{-4} I_p$. All the figures have the same contour levels.

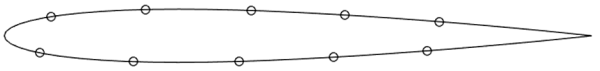

Fig. 6 Location of the pressure measurement points over the surface of a NACA 0009 airfoil.

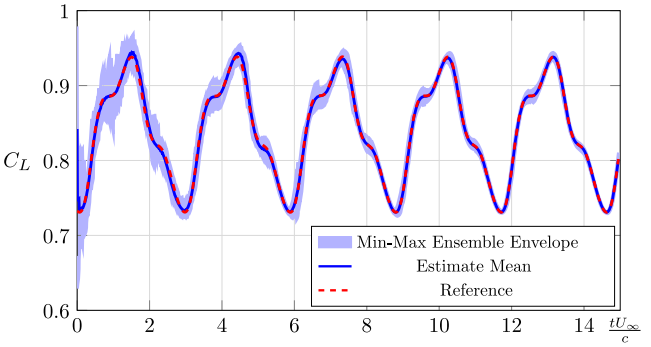

Fig. 7 Estimated lift coefficient for the flow past a NACA 0009 airfoil using pressure measurements and the RTPS covariance inflation scheme ($\theta = 0.95$ and $R = 10^{-4} I_p$).

The relative magnitudes of the measurement influence fields (representers) are now used to iteratively search for the best locations for sensor placement. Starting with a simulation in which measurements are taken at all immersed boundary points, the following methodology was adopted.

1) A simulation is run for T convective time units. At each analysis step, the representers are sorted in descending order by their L_2 norms, and the leading n are selected.

2) A histogram is used to represent how often each representer is selected during the simulation.

3) The n most frequent sensor locations according to the aforementioned histogram are selected.

4) A new simulation is run with only the selected sensor locations, and the process is repeated until the desired number of sensors is achieved.

The length of the simulation T must be chosen carefully. If a small T is chosen, sensor locations more relevant to the filter transient behavior will be favored. A longer simulation length will favor the sensor locations associated with the filter long-term behavior, and the initial filter performance may be hindered. Here, T was set to 20 convective time units, which is about when the estimation statistics reaches its long-term values.

Starting with the first iteration, the regions close to the leading and trailing edges are favored. These regions play an active role in the formation and release of the vortices that characterize this particular flow, and therefore, pressure measurements taken at these locations should be especially effective to determining the state of the system.

The estimated state error, whose norm was previously presented in Fig. 8, is visualized at final instant of the estimation in Fig. 9. Because no modeling errors are present, a global match is achieved even with local measurements after the estimator synchronizes with the reference solution.

B. Estimation in the Presence of Modeling Errors

In practical applications, models are imperfect, and there may be aspects of the dynamics that are not represented in the estimator. As discussed in Sec. II, an explicit stochastic forcing (e.g., via additive covariance inflation) should be the preferred way to mitigate these errors when their source is unknown or hard to be directly modeled. This approach is based on the assumption that their effect can be

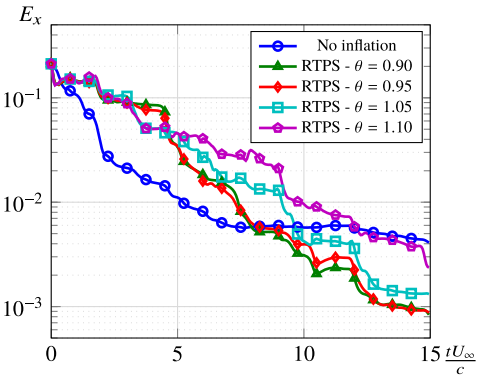

a) State estimate error: Reduction To Prior Spread (RTPS) scheme

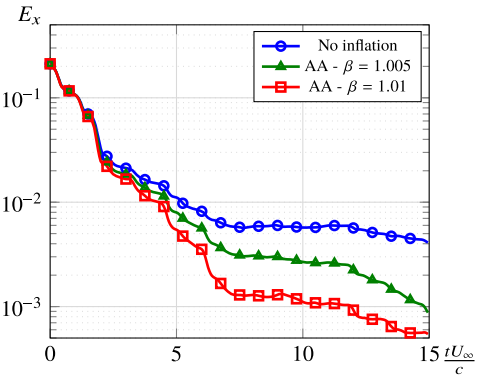

b) State estimate error: Anderson and Anderson (AA) plain multiplicative scheme

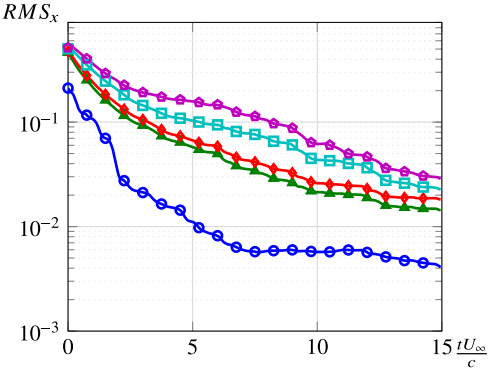

c) Ensemble RMS: Reduction To Prior Spread (RTPS) scheme

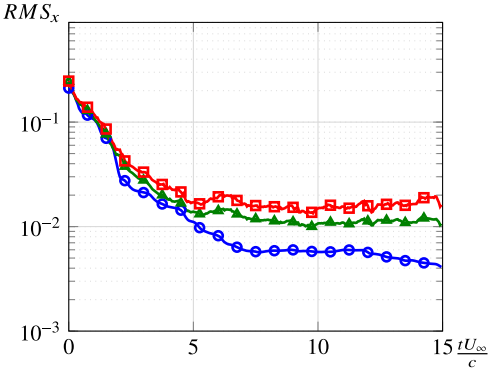

d) Ensemble RMS: Anderson and Anderson (AA) plain multiplicative scheme

Fig. 8 Estimator performance for different multiplicative covariance inflation schemes applied to the flow past a NACA 0009 at high angle of attack. Ensemble size is 24 ($R = 10^{-4}$).

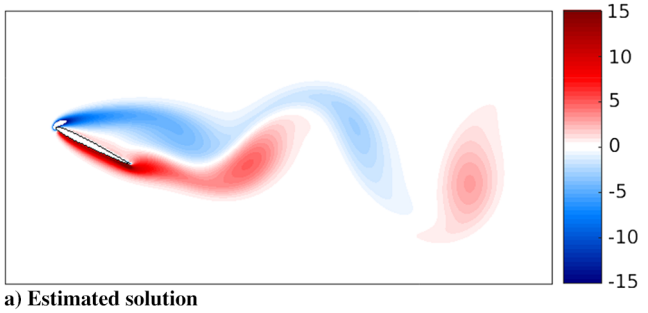

a) Estimated solution

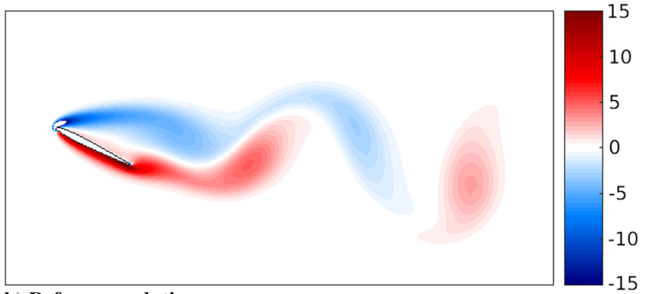

b) Reference solution

Fig. 9 Estimated and reference vorticity field 20 convective time units after estimator initialization using a single pressure sensor optimally placed near the leading edge.

represented by a Gaussian-distributed stochastic forcing with a prescribed mean (often referred as the model bias) and covariance S.

In fields like meteorology, several researchers [44,45] have proposed error covariance models whose corresponding parameters can be tuned online. These models often rely on some low-order representation of these matrices (a popular choice is to use the slow modes of the forecast model). When a suitable representation of these errors in terms of bias and associated covariance is not available, the implementation of this approach becomes impractical. In the absence of a preferential subspace that a low-order representation of the model error covariance matrix would provide, a consistent sampling would require a large ensemble.

A first alternative is what we call the agnostic approach. Any knowledge of the source and structure of the modeling errors is either unknown or ignored. Multiplicative CI is then used to reduce the perceived reliability of the estimator model in comparison with that of the data gathered from sensors. Recall that inflating the ensemble covariance is equivalent to weighting the actual measurements to the detriment of the ones predicted by the estimator internal state [35], allowing more aggressive corrections to the state and enhancing the estimator responsiveness. This approach, however, has limitations. Artificially driving the state toward the measurements usually leads to larger state errors. If the modeling errors are large enough, a closer match in terms of observations may lead to completely unphysical states.

To investigate the capabilities of this approach, the basic framework introduced in Sec. II is maintained, but perturbations are introduced to the freestream velocity of the nature run, affecting both the forecast and measurement evaluations. In a first moment, the reference solution is randomly perturbed by setting the freestream velocity to

$$U_\infty(t) = 1 + 0.1\mathcal{F}_1(\xi(t)) \tag{15}$$

where $\xi(t)$ is a random Gaussian noise sequence, and $\mathcal{F}_1(\cdot)$ is a eighth-order Butterworth filter with a predetermined cutoff reduced frequency fc/U_{ref}. No modification to the estimator model is made other than increasing the multiplicative covariance inflation parameter. The RTPS inflation scheme is chosen over the AA scheme to introduce some variability to the subspace (spanned by the prior ensemble) from which corrections are drawn at each analysis step.

Figure 10 shows the ensemble lift coefficient evolution for two different choices of covariance inflation magnitude and ensemble size. Increasing the former leads to a more aggressive correction behavior, which tends to yield noisier estimates. To some extent, this tendency can be mitigated with a larger ensemble size. A combination of both strategies usually leads to enhanced tracking capabilities.

Provided that the source of the modeling error is known, a second alternative is possible. In the augmentation approach, the goal is to equip the estimator to be able to track the freestream perturbation. We here choose to model the freestream velocity as exhibiting a linear behavior between two consecutive analysis steps, such that the state vector is then augmented [46] with the inclusion of the freestream perturbation and its derivative. The dynamic model for them is a simple integrator with the derivative being propagated as a constant. This approach of simultaneously estimating both state and parameters is often referred to as joint estimation and has the advantage of taking into account the cross-correlation between the state and the parameters.

First, we analyze the performance of the estimator when the airfoil performs a smooth deceleration to 75% of its initial value over 13.3 convective time units so that 87.5% is achieved after 20 convective time units of the beginning of the simulation. The deceleration profile is given by

$$U_\infty(t) = 1 - \frac{\alpha}{2}\text{erfc}\left(-\frac{\sqrt{\pi}\beta}{\alpha}(t - t_0)\right) \tag{16}$$

where $\text{erfc}(t)$ is the complementary error function, α is the saturation value, and β is the slope at $t = t_0$, the reference time at which the perturbation reaches half of its saturation value.

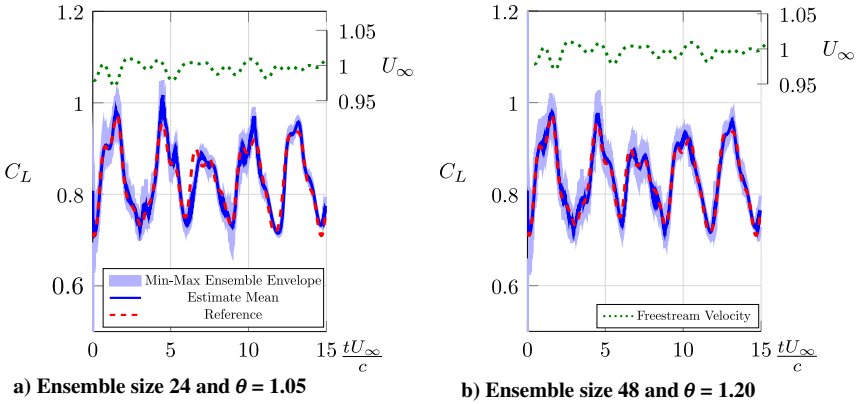

a) Ensemble size 24 and $\theta = 1.05$

b) Ensemble size 48 and $\theta = 1.20$

Fig. 10 Estimated lift coefficient for airfoil with randomized freestream velocity using the RTPS covariance inflation scheme ($R = 10^{-4}I_p$)

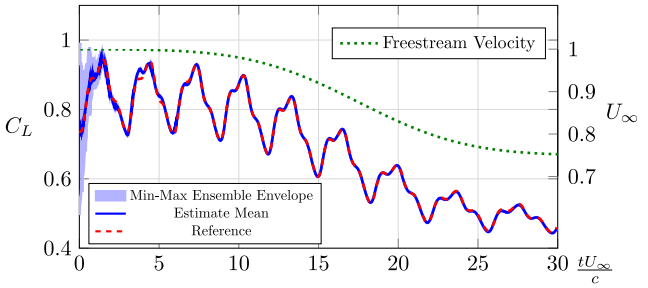

Fig. 11 Estimated lift coefficient for decelerating airfoil using the RTPS ($\theta = 0.9$) covariance inflation scheme and $R = 10^{-6} I_p$.

Figure 11 shows some interesting features of the EnKF. Because the IB forces acting on the body are a function of the vorticity field as well as the freestream velocity and acceleration, the lift (the sum of the vertical components of these forces) is a good global performance indicator for this estimation problem. For early times, the C_L ensemble variance is larger than the perfect model case due to the extra degree of uncertainty added by the presence of a perturbation of unknown magnitude, but the estimator is able to obtain the right phase after just two convective time units, and most of the perturbation tracking is performed while the estimator has already a good estimate for the state of the system.

Figure 12 shows how the parameters estimate evolves with an increasing inflation magnitude. For early times, the poorer estimates are consistent with the transient behavior that was observed in Fig. 11. The impact of the covariance inflation parameter is more pronounced in the acceleration, in which higher values lead to a better overall tracking but noisier initial estimates.

If the same deceleration is performed over a single convective time unit, keeping all other parameters the same, the performance of the estimator degrades (see Fig. 13). The reason here is the fact that the freestream velocity only changes after 19 convective time units after the beginning of the simulation, when the estimator internal variance already reached its lower limit and the responsiveness of the estimator to external changes is already low (dashed line in Fig. 14). Therefore, it is necessary that the innovation norm grows before the estimator responds accordingly leading to the significant response delay observed in Fig. 13. Increasing the multiplicative covariance inflation would help to delay the variance decay, but its effectiveness will be directly linked to the size interval between the beginning of the estimation and the deceleration event. Also, a multiplicative covariance inflation that is too high will lead to noisier estimates for early estimation times.

Alternatively, one could stochastically force the parameters dynamics to keep their variance in a level that is high enough to ensure responsiveness. For this particular problem, we choose to force the disturbance derivative with a zero-mean Gaussian-distributed random quantity with a variance level one order of magnitude below the maximum expected derivative level so that the parameters ensemble covariance is kept above a minimum threshold (see solid line in Fig. 14). Figure 13 shows that this addition enhances the estimator tracking performance.

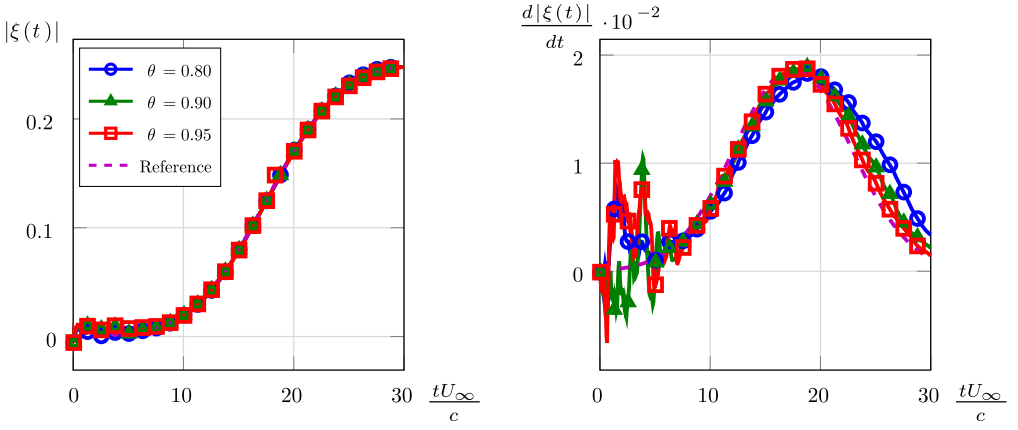

a) Free stream velocity perturbation **b) Free stream velocity perturbation derivative**

Fig. 12 Joint parameter/state estimation for an airfoil decelerating to 75% of its initial value over 13.3 convective time units for different covariance inflation levels. The measurement noise level is set to $R = 10^{-6} I_p$.

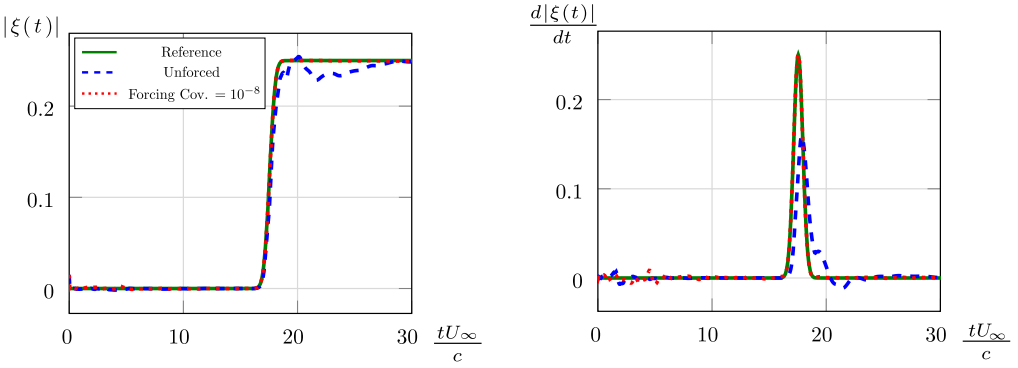

a) Free stream velocity perturbation **b) Free stream velocity perturbation derivative**

Fig. 13 Joint parameter/state estimation for an airfoil decelerating to 75% of its initial value over one convective time unit ($R = 10^{-6} I_p$,$\theta = 0.90$). Forced parameter dynamics enhances estimator responsiveness.

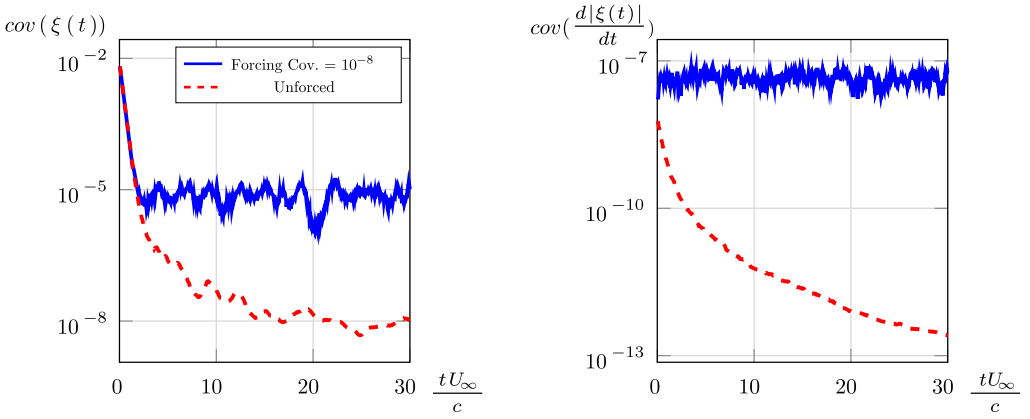

a) Free stream velocity perturbation **b) Free stream velocity perturbation derivative**

Fig. 14 Influence of an explicit stochastic forcing on the evolution of the estimated parameters covariance for an airfoil decelerating to 75% of its initial value over one convective time unit ($R = 10^{-6} I_p, \theta = 0.90$).

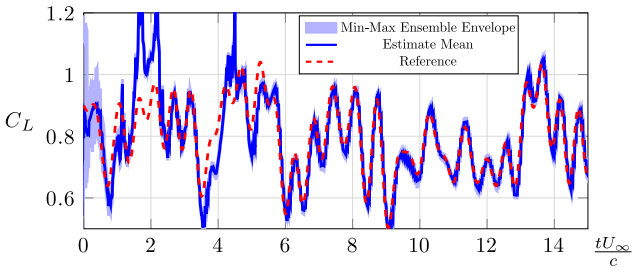

Fig. 15 Estimated lift coefficient for an airfoil subjected to random freestream perturbation (reduced cutoff frequency is two) using the RTPS covariance inflation scheme ($\theta = 0.9$, $R = 10^{-6} I_p$).

The same methodology can be applied to the random freestream perturbation case. Figures 15 and 16 show the estimator performance when the freestream velocity is randomly perturbed (cutoff frequency is 2). Different from the deceleration case, the perturbations are already present at the beginning of the simulation, and the estimator must be able to filter out the effects of the unknown initial condition while tracking the changes in the freestream. This fact accounts for the longer transient that the estimator experiences. Again, the explicit stochastic forcing plays a fundamental role in keeping the estimator responsive to changes in the freestream velocity at late estimation times.

IV. Conclusions

In this paper, a dual-experiment methodology, in which the numerical algorithm is used as both the estimator and as a surrogate for the measurements, was employed to investigate the performance of an EnKF-based estimator for aerodynamic problems. The estimator was demonstrated to provide a framework that combines the fidelity and robustness of a high-dimensional representation of the dynamical system with the computational efficiency of a low-order approximation of the state covariance.

A reduced number of either velocity or pressure measurements were successfully used to estimate the phase of the vortex shedding, and thus the corresponding forces, in flow past a cylinder or an airfoil. In terms of performance, global measurements, such as the velocity in the wake, are more efficient in constraining the flow state. Estimation based on local measurements, such as pressure on the surface, results in longer transients before achieving the same state error level. However, using pressure measurements makes the estimator more responsive in tracking the forces acting on the body, which is especially desirable when freestream perturbations are present.

For flows where the dynamics evolve on a relatively small manifold, the results indicate that correspondingly small ensemble sizes are sufficient to provide a suitable representation of the covariance matrix and lead to an asymptotic behavior of the estimator dynamics.

An analysis of the measurement's influence fields (the so-called representers) provided interesting a posteriori information about those measurements that were most effective during the filtering

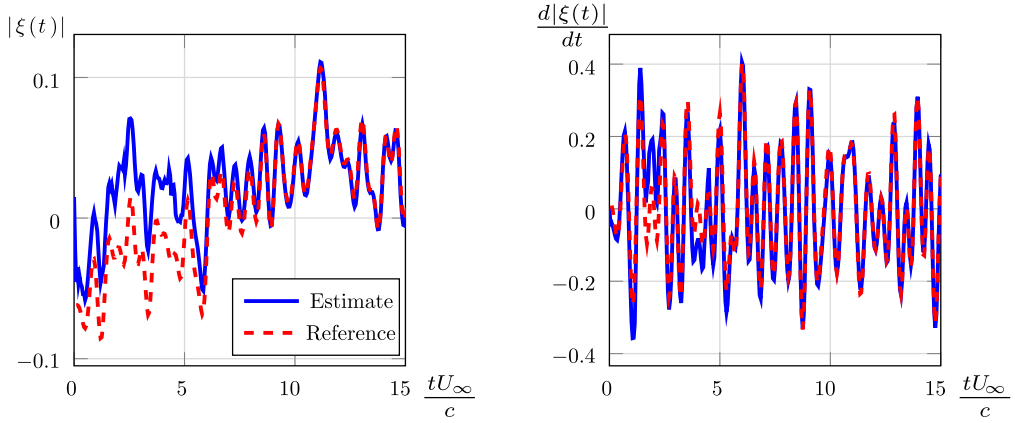

a) Free stream velocity perturbation **b) Free stream velocity perturbation derivative**

Fig. 16 Joint parameter/state estimation for an airfoil subjected to random freestream perturbations (reduced cutoff frequency is two) using the RTPS inflation scheme ($\theta = 0.90$, $R = 10^{-6} I_p$).

process. Thus, the representers provide useful guidance on sensor placement. In the cylinder case, the region of highest influence was coincident with the wave-maker region as predicted by structural sensitivity analysis. In the airfoil case, pressure measurements taken close to leading and trailing edges are most effective in the estimation process.

Through the successive application of Kalman's analysis step, the estimated system covariance is bound to decrease until it reaches a level (determined by the measurement noise level) at which new measurements have little impact. The distinctive behavior shown in Fig. 4 highlights the dynamic balance between the reliability of the internal state and the measurement uncertainty. Multiplicative covariance inflation was then used with two objectives: to delay the covariance collapse induced by the reduced ensemble size, and to increase the weight of the measurements in the presence of unmodeled forecast errors.

Alternatively, when the source of the forecast errors is known, parametric modeling can be used to upgrade the estimator model. The parameters and state variables can be jointly estimated by using an augmented state-vector approach. Additive process noise can be introduced to ensure the responsiveness of the estimator for later simulation times. Using this approach, with a linear representation for the freestream velocity, both the flow state and the lift were successfully estimated for an airfoil exposed to an unknown freestream velocity perturbation. Under a deterministic deceleration, the estimator accurately captured a steep change in the freestream velocity (25% reduction of the initial velocity over one convective time unit). When subjected to a sequence of random gusts (reduced frequency up to 2 and amplitude up to 10% of the reference velocity), the estimator was able to achieve synchronization after a transient period of about 10 convective time units.

Acknowledgments

This work has been supported in part by a grant from the U.S. Air Force Office of Scientific Research (FA9550-14-1-0328) with Douglas Smith as program manager. A. F. C. da Silva would like to thank the Ministry of Education of Brazil (Capes Foundation) for its support through a Science Without Borders scholarship (grant BEX 12966/13-4). The authors also acknowledge Andrew Stuart (California Institute of Technology), David Williams (Illinois Institute of Technology), and Jeff Eldredge (University of California, Los Angeles) for helpful discussions of this work.

References

[1] Brunton, S. L., and Noack, B. R., "Closed-Loop Turbulence Control: Progress and Challenges," *Applied Mechanics Reviews*, Vol. 67, No. 5, 2015, Paper 050801. doi:10.1115/1.4031175

[2] Kalman, R. E., and Bucy, R. S., "New Results in Linear Filtering and Prediction Theory," *Journal of Basic Engineering*, Vol. 83, No. 1, 1961, pp. 95–108. doi:10.1115/1.3658902

[3] Hayase, T., Nisugi, K., and Shirai, A., "Numerical Realization for Analysis of Real Flows by Integrating Computation and Measurement," *International Journal for Numerical Methods in Fluids*, Vol. 47, Nos. 6–7, 2005, pp. 543–559. doi:10.1002/(ISSN)1097-0363

[4] Gerhard, J., Pastoor, M., King, R., Noack, B. R., Dillmann, A., Morzynski, M., and Tadmor, G., "Model-Based Control of Vortex Shedding Using Low-Dimensional Galerkin Models," *33rd AIAA Fluid Dynamics Conference and Exhibit*, AIAA Paper 2003-4262, June 2003. doi:10.2514/6.2003-4262

[5] Aleksic, K., Luchtenburg, M., King, R., Noack, B. R., and Pfeiffer, J., "Robust Nonlinear Control Versus Linear Model Predictive Control of a Bluff Body Wake," *5th AIAA Flow Control Conference*, AIAA Paper 2010-4833, June–July 2010. doi:10.2514/6.2010-4833.

[6] Ahuja, S., and Rowley, C. W., "Feedback Control of Unstable Steady States of Flow past a Flat Plate Using Reduced-Order Estimators," *Journal of Fluid Mechanics*, Vol. 645, Feb. 2010, p. 447. doi:10.1017/S0022112009992655

[7] Flinois, T. L. B., and Morgans, A. S., "Feedback Control of Unstable Flows: A Direct Modelling Approach Using the Eigensystem Realisation Algorithm," *Journal of Fluid Mechanics*, Vol. 793, April 2016, pp. 41–78. doi:10.1017/jfm.2016.111

[8] Fukumori, I., and Malanotte-Rizzoli, P., "An Approximate Kalman Filter for Ocean Data Assimilation: An Example with an Idealized Gulf Stream Model," *Journal of Geophysical Research: Oceans*, Vol. 100, No. C4, 1995, pp. 6777–6793. doi:10.1029/94JC03084

[9] Suzuki, T., "Reduced-Order Kalman-Filtered Hybrid Simulation Combining Particle Tracking Velocimetry and Direct Numerical Simulation," *Journal of Fluid Mechanics*, Vol. 709, Oct. 2012, pp. 249–288. doi:10.1017/jfm.2012.334

[10] Evensen, G., *Data Assimilation: The Ensemble Kalman Filter*, 1st ed., Springer Science & Business Media, Berlin, 2009, pp. 163–167.

[11] Kalnay, E., *Atmospheric Modeling, Data Assimilation and Predictability*, Cambridge Univ. Press, Cambridge, England, U.K., 2003.

[12] Colburn, C. H., Cessna, J. B., and Bewley, T. R., "State Estimation in Wall-Bounded Flow Systems. Part 3. The Ensemble Kalman Filter," *Journal of Fluid Mechanics*, Vol. 682, Sept. 2011, pp. 289–303. doi:10.1017/jfm.2011.222

[13] Kikuchi, R., Misaka, T., and Obayashi, S., "Assessment of Probability Density Function Based on POD Reduced-Order Model for Ensemble-Based Data Assimilation," *Fluid Dynamics Research*, Vol. 47, No. 5, 2015, Paper 051403. doi:10.1088/0169-5983/47/5/051403

[14] Kato, H., Yoshizawa, A., Ueno, G., and Obayashi, S., "A Data Assimilation Methodology for Reconstructing Turbulent Flows Around Aircraft," *Journal of Computational Physics*, Vol. 283, Feb. 2015, pp. 559–581. doi:10.1016/j.jcp.2014.12.013

[15] Mons, V., Chassaing, J.-C., Gomez, T., and Sagaut, P., "Reconstruction of Unsteady Viscous Flows Using Data Assimilation Schemes," *Journal of Computational Physics*, Vol. 316, July 2016, pp. 255–280. doi:10.1016/j.jcp.2016.04.022

[16] Lorenc, A. C., "Analysis Methods for Numerical Weather Prediction," *Quarterly Journal of the Royal Meteorological Society*, Vol. 112, No. 474, 1986, pp. 1177–1194. doi:10.1002/(ISSN)1477-870X

[17] Stengel, R. F., *Optimal Control and Estimation*, Courier Corp., New York, 2012, p. 342.

[18] Gillijns, S., Mendoza, O. B., Chandrasekar, J., De Moor, B. L. R., Bernstein, D. S., and Ridley, A., "What Is the Ensemble Kalman Filter and How Well Does It Work?" *Proceedings of the 2006 American Control Conference*, IEEE Publ., Piscataway, NJ, 2006, pp. 4448–4453. doi:10.1109/ACC.2006.1657419

[19] Gelb, A., *Applied Optimal Estimation*, MIT Press, Cambridge, MA, 1974, pp. 180–202.

[20] Julier, S. J., and Uhlmann, J. K., "Unscented Filtering and Nonlinear Estimation," *Proceedings of the IEEE*, Vol. 92, No. 3, 2004, pp. 401–422. doi:10.1109/JPROC.2003.823141

[21] Wan, E. A., and Van Der Merwe, R., "The Unscented Kalman Filter for Nonlinear Estimation," *Proceedings of the IEEE 2000 Adaptive Systems for Signal Processing, Communications, and Control Symposium*, IEEE Publ., Piscataway, NJ, 2000, pp. 153–158. doi:10.1109/ASSPCC.2000.882463

[22] van Leeuwen, P. J., "Particle Filtering in Geophysical Systems," *Monthly Weather Review*, Vol. 137, No. 12, 2009, pp. 4089–4114. doi:10.1175/2009MWR2835.1

[23] Bellman, R. E., *Dynamic Programming*, Dover, New York, 2003, p. IX.

[24] Evensen, G., "Sequential Data Assimilation with a Nonlinear Quasi-Geostrophic Model Using Monte Carlo Methods to Forecast Error Statistics," *Journal of Geophysical Research: Oceans*, Vol. 99, No. C5, 1994, pp. 10143–10162. doi:10.1029/94JC00572

[25] Bengtsson, T., Snyder, C., and Nychka, D., "Toward a Nonlinear Ensemble Filter for High-Dimensional Systems," *Journal of Geophysical Research: Atmospheres*, Vol. 108, No. D24, 2003, pp. 1–10. doi:10.1029/2002JD002900

[26] Evensen, G., "Sampling Strategies and Square Root Analysis Schemes for the EnKF," *Ocean Dynamics*, Vol. 54, No. 6, 2004, pp. 539–560. doi:10.1007/s10236-004-0099-2

[27] Anderson, J. L., and Anderson, S. L., "A Monte Carlo Implementation of the Nonlinear Filtering Problem to Produce Ensemble Assimilations and Forecasts," *Monthly Weather Review*, Vol. 127, No. 12, 1999, pp. 2741–2758. doi:10.1175/1520-0493(1999)127<2741:AMCIOT>2.0.CO;2

[28] Papadakis, N., Mémin, É., Cuzol, A., and Gengembre, N., "Data Assimilation with the Weighted Ensemble Kalman Filter," *Tellus A*, Vol. 62, No. 5, 2010, pp. 673–697. doi:10.1111/j.1600-0870.2010.00461.x

[29] Nerger, L., Hiller, W., and Schröter, J., "A Comparison of Error Subspace Kalman Filters," *Tellus A*, Vol. 57, No. 5, 2005, pp. 715–735. doi:10.3402/tellusa.v57i5.14732

[30] Evensen, G., and Van Leeuwen, P. J., "Assimilation of Geosat Altimeter Data for the Agulhas Current Using the Ensemble Kalman Filter with a Quasigeostrophic Model," *Monthly Weather Review*, Vol. 124, No. 1, 1996, pp. 85–96. doi:10.1175/1520-0493(1996)124<0085:AOGADF>2.0.CO;2

[31] Lawson, W. G., and Hansen, J. A., "Implications of Stochastic and Deterministic Filters as Ensemble-Based Data Assimilation Methods in Varying Regimes of Error Growth," *Monthly Weather Review*, Vol. 132, No. 8, 2004, pp. 1966–1981. doi:10.1175/1520-0493(2004)132<1966:IOSADF>2.0.CO;2

[32] Le Gland, F., Monbet, V., and Tran, V.-D., "Large Sample Asymptotics for the Ensemble Kalman Filter," Rept. RR-7014, Institut National de Recherche en Informatique et en Automatique, Rennes, France, 2009.

[33] Evensen, G., "The Ensemble Kalman Filter: Theoretical Formulation and Practical Implementation," *Ocean Dynamics*, Vol. 53, No. 4, 2003, pp. 343–367. doi:10.1007/s10236-003-0036-9

[34] van Leeuwen, P. J., "Comment on 'Data Assimilation Using an Ensemble Kalman Filter Technique'," *Monthly Weather Review*, Vol. 127, No. 6, 1999, pp. 1374–1377. doi:10.1175/1520-0493(1999)127<1374:CODAUA>2.0.CO;2

[35] Kelly, D., Law, K., and Stuart, A. M., "Well-Posedness and Accuracy of the Ensemble Kalman Filter in Discrete and Continuous Time," *Nonlinearity*, Vol. 27, No. 10, 2014, pp. 2579–2603. doi:10.1088/0951-7715/27/10/2579

[36] Whitaker, J. S., and Hamill, T. M., "Evaluating Methods to Account for System Errors in Ensemble Data Assimilation," *Monthly Weather Review*, Vol. 140, No. 9, 2012, pp. 3078–3089. doi:10.1175/MWR-D-11-00276.1

[37] Sacher, W., and Bartello, P., "Sampling Errors in Ensemble Kalman Filtering. Part 1: Theory," *Monthly Weather Review*, Vol. 136, No. 8, 2008, pp. 3035–3049. doi:10.1175/2007MWR2323.1

[38] Taira, K., and Colonius, T., "The Immersed Boundary Method: A Projection Approach," *Journal of Computational Physics*, Vol. 225, No. 2, 2007, pp. 2118–2137. doi:10.1016/j.jcp.2007.03.005

[39] Colonius, T., and Taira, K., "A Fast Immersed Boundary Method Using a Nullspace Approach and Multi-Domain Far-Field Boundary Conditions," *Computer Methods in Applied Mechanics and Engineering*, Vol. 197, No. 25, 2008, pp. 2131–2146. doi:10.1016/j.cma.2007.08.014

[40] Liska, S., and Colonius, T., "A Parallel Fast Multipole Method for Elliptic Difference Equations," *Journal of Computational Physics*, Vol. 278, Dec. 2014, pp. 76–91. doi:10.1016/j.jcp.2014.07.048

[41] Liska, S., and Colonius, T., "A Fast Immersed Boundary Method for External Incompressible Viscous Flows Using Lattice Green's Functions," *Journal of Computational Physics*, Vol. 331, Feb. 2017, pp. 257–279. doi:10.1016/j.jcp.2016.11.034

[42] Williamson, C. H. K., "The Existence of Two Stages in the Transition to Three-Dimensionality of a Cylinder Wake," *Physics of Fluids*, Vol. 31, No. 11, 1988, pp. 3165–3168. doi:10.1063/1.866925

[43] Giannetti, F., and Luchini, P., "Structural Sensitivity of the First Instability of the Cylinder Wake," *Journal of Fluid Mechanics*, Vol. 581, 2007, pp. 167–197. doi:10.1017/S0022112007005654

[44] Dee, D. P., "On-Line Estimation of Error Covariance Parameters for Atmospheric Data Assimilation," *Monthly Weather Review*, Vol. 123, No. 4, 1995, pp. 1128–1145. doi:10.1175/1520-0493(1995)123<1128:OLEOEC>2.0.CO;2

[45] Cohn, S. E., and Parrish, D. F., "The Behavior of Forecast Error Covariances for a Kalman Filter in Two Dimensions," *Monthly Weather Review*, Vol. 119, No. 8, 1991, pp. 1757–1785. doi:10.1175/1520-0493(1991)119<1757:TBOFEC>2.0.CO;2

[46] Anderson, J. L., "An Ensemble Adjustment Kalman Filter for Data Assimilation," *Monthly Weather Review*, Vol. 129, No. 12, 2001, pp. 2884–2903. doi:10.1175/1520-0493(2001)129<2884:AEAKFF>2.0.CO;2

H. Blackburn
Associate Editor